Spectrochimica Acta Part A: Molecular and Biomolecular Spectroscopy 207 (2019) 328–336

Contents lists available at ScienceDirect

Spectrochimica Acta Part A: Molecular and Biomolecular Spectroscopy

journal homepage: www.elsevier.com/locate/saa

Rotamers of *p* isopropylphenol studied by hole-burning resonantly enhanced multiphoton ionization and mass analyzed threshold ionization spectroscopy

Yan Zhao [a], Yinghui Jin [a], Jiayu Hao [a], Yonggang Yang [a,b], Lirong Wang [a,b], Changyong Li [a,b,*], Suotang Jia [a,b]

[a] State Key Laboratory of Quantum Optics and Quantum Optic Devices, Institute of Laser Spectroscopy, Shanxi University, Taiyuan, Shanxi 030006, China
[b] Collaborative Innovation Center of Extreme Optics, Shanxi University, Taiyuan, Shanxi 030006, China

ARTICLE INFO

Article history:
Received 27 June 2018
Received in revised form 5 September 2018
Accepted 8 September 2018
Available online 10 September 2018

Keywords:
p isopropylphenol
Mass analyzed threshold ionization
Hole-burning spectroscopy
Density functional theory
Spectral simulation

ABSTRACT

The resonance enhanced multiphoton ionization (REMPI), ultraviolet-ultraviolet (UV-UV) hole burning and mass analyzed threshold ionization (MATI) spectroscopy have been applied to investigate the vibrational features of *p* isopropylphenol in its first electronically excited state S_1 and cationic ground state D_0. Two stable conformational structures of *p* isopropylphenol are distinctly found in the supersonic molecular beam and identified as the *cis* and *trans* rotamers through REMPI and UV-UV hole burning spectroscopy. The electronic excitation energies of $S_1 \leftarrow S_0$ transition of two rotamers are determined to be 35,578 and 35,593 cm^{-1}, and the adiabatic ionization energies are 65,331 and 65,350 cm^{-1}, respectively. The MATI spectra recorded via different intermediate levels of S_1 state indicate the similarity in the molecular geometry between the S_1 state and the D_0 state for each rotamer of *p* isopropylphenol. Geometrical optimizations of *p* isopropylphenol have also been performed using the density functional theory (DFT) for S_0 and D_0 states, and time-dependent density functional theory (TDDFT) for S_1 state. The simulated spectra for $S_1 \leftarrow S_0$ and $D_0 \leftarrow S_1$ transitions of two rotamers are able to reproduce qualitatively the experimental spectral profile, which help us to assign the vibronic modes. Most of the observed vibrations of two rotamers in the S_1 and D_0 states are related to the in-plane ring deformation and some active modes involving isopropyl group.

1. Introduction

The spectroscopy of the phenol and substituted phenols in the gas phase is popular topic of theoretical and experimental studies with the aim to understand their photochemical and photophysical properties, such as the photodissociation dynamics [1–4], and noncovalent interactions [5,6]. Furthermore, these investigations can also provide valuable information on the many chemical and biological processes because phenol is the chromophore site in several biologically active molecules including the amino acid tyrosine and the estrogenic hormones [7–9]. The vibronic spectra and geometrical structures of some *para*-alkyl phenols in the first electronically excited S_1 and cationic ground D_0 states have been the topic of several experimental and theoretical studies. For these molecules, alkyl is an electron-donor group that introduces the electronic charge in the π orbital of the aromatic ring by the hyperconjugation, resulting in a change of the electron density distribution of the molecule [3]. The resonance enhanced multiphoton ionization (REMPI), laser induced fluorescence (LIF) excitation, dispersed fluorescence, autoionization-detected infrared (ADIR), and mass analyzed threshold ionization (MATI) spectroscopy have been applied to study *p* methylphenol, *p* ethylphenol, and *p n* propylphenol [6,10–15]. Several *p* methylphenol water cluster [14,16], *p* methylphenol NH_3 H_2O complex [17–19], *p* methylphenol *p* aminophenol heterodimer [20], and *p* ethylphenol Ar cluster [21] have also been studied for exploring the intermolecular interaction. In contrast, the detailed spectral information of *p* isopropylphenol in the S_1 and D_0 states is still limited.

Several studies of the physical and chemical properties of *p* isopropylphenol have been carried out over the past several decades. Szostak et al. reported the infrared, Raman and UV–Vis spectra of *p* isopropylphenol in the solid and solution in order to understand the nonlinear optical property of the crystal [22]. Wojcik and Holband explored the structural changes and intermolecular interactions of crystalline *p* isopropylphenol at several temperatures by Raman scattering, inelastic neutron scattering, and X-ray diffraction experiments [23]. The LIF spectrum of *p* isopropylphenol in the gas phase was reported by Song and Hayes, and only a few of vibrational bands in the S_1 state were assigned [11]. They suspected that there may be two stable rotamers for *p* isopropylphenol due to a doublet origin structure found in the LIF spectra. With the theoretical calculations at the MP2/6-31G (d,p) level, Jones's group predicted two stable rotamer structures of

* Corresponding author at: State Key Laboratory of Quantum Optics and Quantum Optic Devices, Institute of Laser Spectroscopy, Shanxi University, Taiyuan, Shanxi 030006, China.
E-mail address: lichyong@sxu.edu.cn (C. Li).

https://doi.org/10.1016/j.saa.2018.09.013
1386-1425/

p isopropylphenol in its ground electronic state S_0 [24], here we named them as *trans* and *cis* rotamers depending on the orientation of the isopropyl group with respect to the hydrogen group, as shown in Fig. 1. However, the molecular crystal structure from X-ray diffraction shows that there is only one *trans* rotamer of *p* isopropylphenol at room temperature [25]. The UV-UV hole burning spectroscopy with a supersonic jet-cooled expansion is one of the most powerful tools for the study on rotamer in the gas phase, which can easily determinate the variety of rotamers and distinguish the vibronic transitions in the REMPI spectrum from each rotamer [26–30]. In this paper we report the one-color resonance enhanced two-photon ionization (R2PI) and UV-UV hole burning spectra of *p* isopropylphenol to identify the rotamers and distinguish their vibronic transitions in the first excited state S_1. The adiabatic ionization energy and cationic vibronic features were obtained by MATI [31] spectroscopy, which is based on the same principle as ZEKE [32,33] except for the difference that the ZEKE detects electrons and the MATI detects ions. The REMPI and MATI spectra were simulated by Frank-Condon approach to help to assign the observed bands in S_1 and D_0 states.

2. Experimental and Computational Details

2.1. Experimental Method

The experimental apparatus employed in this paper was a supersonic molecular beam time-of-flight spectrometer combined with two tunable dye lasers [34]. *p* isopropylphenol was purchased from MACKLIN (98% purity) and used without further purification. The sample was heated to approximately 100 °C to obtain a sufficient vapor pressure. In order to generate the supersonic molecular beam, the sample vapors were seeded in 2 bar of argon and expanded into the vacuum chamber through a pulsed valve (Parker valve) with a nozzle orifice of 0.5 mm in diameter, which operated at a repetition rate of 10 Hz with the pulse duration of 210 μs. A 1 mm diameter skimmer located at about 20 mm downstream from the nozzle orifice was applied to collimate the molecular beam. During the experiments, the expansion and ionization regions were maintained at a pressure of about 1.1×10^{-4} and 1.6×10^{-6} Pa, respectively.

The one-color R2PI spectrum of *p* isopropylphenol was recorded by scanning the tunable UV excitation laser in the 274–282 nm, which was generated by a frequency-doubled dye laser (Sirah CBR-D-24 with BBO crystal, Coumarin 540A dye) pumped by a third harmonic of a Nd: YAG laser (Quanta-Ray INDI-40-10: 355 nm). In order to confirm the variety of the rotamers and investigate the spectral features in the R2PI spectrum, we measured the UV-UV hole-burning spectra of *p* isopropylphenol using a second frequency-doubled dye laser (Sirah PrecisionScan-D with BBO crystal, Coumarin 540A dye) as a hole-burning laser, which is pumped by a third harmonic of a Nd: YAG laser (Quantel Q-smart 850: 355 nm). The wavelength of probe laser (excitation laser) was fixed to a resonant transition of a rotamer, while the hole-burning laser was scanned with a time advance of 150 ns. When the hole-burning laser was resonant with the rotamer selected by the probe laser, it caused a decrease in the R2PI signals of the probe laser. Thus, by monitoring the signal of the probe laser, the hole-burning spectrum involving vibronic bands of a single specific rotamer can be obtained [26,35]. Both counter-propagating UV lasers were operated at 10 Hz and perpendicularly intersected with the molecular beam. The absolute wavelengths of both lasers were calibrated with a wavelength meter (HighFinesse WS-7).

In the two-color MATI experiments, the pump laser was fixed to a specific vibronic transition of $S_1 \leftarrow S_0$, while the probe laser was scanned to populate excited molecule to long-lived high *n* Rydberg states. About 200 ns after lasers, a weak pulse electric field of −1.3 V/cm was applied to move the prompt ions towards the opposite direction to the detector. The Rydberg molecules kept moving and then were ionized and accelerated by two pulse electric fields of 140 V/cm and 570 V/cm. The threshold ions passed a 48 mm field-free region and were detected by a dual-stack microchannel plate (MCP) detector. A multichannel scaler (MCS, Stanford Research Systems, SR430) interfaced to a computer was used to collect and analyze the ion signal from the detector. Each mass spectrum was accumulated for 300 laser shots.

2.2. Computational Method

In order to investigate the vibrational features in the R2PI, hole-burning and MATI spectra of *p* isopropylphenol, we used the Gaussian 09 program package [36] to optimize the molecular structures and calculate the harmonic vibrational frequencies for all the involved electronic states of *p* isopropylphenol. For the electronic ground state (S_0) and the cationic ground state (D_0), the density functional theory (DFT) calculations using the B3LYP functional were performed with the aug-cc-pVDZ basis set. The first electronically excited state (S_1) was calculated using the time dependent density functional theory (TDDFT) with the B3LYP functional. Since the vibrational frequency calculations were based on the harmonic oscillator model, the calculated frequencies were scaled by a factor to approximately correct for the deviations arising from the neglect of anharmonic effects, the incomplete treatment of electron correlation and the use of a finite basis set [37,38]. All calculated frequencies and scaling factors were listed in Tables 2–4 together with the experimental results. On the basis of the above calculations, the vibrationally resolved electronic spectra of *p* isopropylphenol for $S_1 \leftarrow S_0$ and $D_0 \leftarrow S_1$ transitions were simulated using the Gaussian 09 program under the Franck-Condon approximation [36].

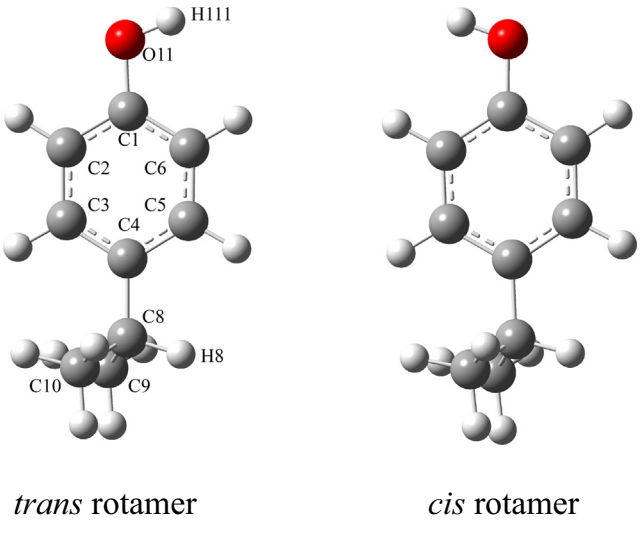

Fig. 1. Molecular structures of *trans* and *cis* rotamers of *p* isopropylphenol.

3. Results

3.1. Molecular Structure of p isopropylphenol

The different initial geometries of *p* isopropylphenol in S_0 state have been optimized without any constraint at the B3LYP/aug-cc-pVDZ level. Two stable structures were obtained as shown in Fig. 1, which is consistent with the previous results at the MP2/6-31G(d,p) level [24]. The C_8—H_8 bond and hydroxyl group lie in the plane of aromatic ring, and two methyl groups of the isopropyl group are located on both sides of the plane of the aromatic ring. The optimized geometrical parameters for the S_0 state of *p* isopropylphenol together with the experimental data [25] obtained from the crystallographic X-ray diffraction are listed in Table 1. For the S_0 state of *trans* rotamer, the theoretical bond lengths and bond angles are in good agreement with the experimental values

Table 1
Geometrical parameters of *p* isopropylphenol in its electronic ground and excited states.

	trans				*cis*		$\Delta(S_1\text{-}S_0)$	
	Exp.[a]	Ref.22[b]	S_0[c]	S_1[d]	S_0[c]	S_1[d]	*trans*	*cis*
Bond length (Å)								
C_1—C_2	1.384	1.422	1.399	1.417	1.400	1.428	0.018	0.028
C_2—C_3	1.395	1.423	1.394	1.420	1.397	1.421	0.024	0.024
C_3—C_4	1.397		1.406	1.430	1.403	1.430	0.024	0.027
C_4—C_5	1.366		1.400	1.427	1.403	1.426	0.027	0.026
C_5—C_6	1.399	1.423	1.398	1.419	1.397	1.421	0.021	0.024
C_6—C_1	1.362	1.422	1.398	1.430	1.397	1.419	0.032	0.022
C_1—O_{11}	1.395	1.429	1.374	1.348	1.374	1.349	−0.026	−0.025
O_{11}—H_{111}	0.88	0.984	0.965	0.975	0.965	0.974	0.010	0.009
C_4—C_8	1.516	1.541	1.522	1.507	1.522	1.507	−0.015	−0.015
C_8—H_{81}	0.96	1.109	1.101	1.100	1.101	1.100	−0.001	−0.001
C_8—C_9	1.520	1.566	1.540	1.546	1.540	1.546	0.006	0.006
C_8—C_{10}	1.500	1.566	1.540	1.544	1.540	1.545	0.004	0.005
Angle(deg)								
$C_1C_2C_3$	119.6	119.4	119.7	118.4	119.5	117.6	−1.3	−1.9
$C_2C_3C_4$	120.9		121.8	119.8	121.9	120.3	−2.0	−1.6
$C_3C_4C_5$	117.8		117.4	120.4	117.3	120.5	3.0	3.2
$C_4C_5C_6$	121.6		121.7	120.7	121.6	120.2	−1.0	−1.4
$C_5C_6C_1$	120.1	119.4	119.7	117.3	119.9	118.0	−2.4	−1.9
$C_6C_1C_2$	119.8	120.4	119.7	123.2	119.7	123.3	3.5	3.6
$C_4C_8H_{81}$	102.0	106.9	106.7	107.2	106.7	107.1	0.5	0.4
$C_1O_{11}H_{111}$	105.0	111.2	109.5	109.2	109.5	109.3	−0.3	−0.2

[a] Experimental data of *trans* rotamer from Ref [25].
[b] MP2/D95V calculation.
[c] B3LYP/Aug-cc-pVDZ calculation.
[d] TD-B3LYP/Aug-cc-pVDZ calculation.

[25] and are better than the previous MP2/D95V calculation [22]. For example, C—C bond lengths and all CCC angels of benzene ring are similar to the experimental values, and the bond lengths of C_2—C_3 (1.394 Å) and C_5—C_6 (1.398 Å) are very close to the experimental ones (1.394 and 1.399 Å). The C_1—O_{11} bond length (1.374 Å) is closer to the experimental value (1.395 Å) than the previous theoretical result (1.429 Å). The bond lengths of C_4—C_8 (1.522 Å) and C_8—C_9 (1.540 Å) are slightly overestimated by 0.006 and 0.020 Å with respect to the experimental values 1.516 and 1.520 Å, respectively. The deviations between the calculated and experimentally observed bond lengths and bond angles mainly result from O_{11}—H_{111} bond (0.965 Å) and C_1—O_{11}—H_{111} angle (109.5°), which are overestimated by 0.085 Å and 4.5°. This is probably caused by the intermolecular interactions between the crystalline *p* isopropylphenol and the hydrogen-bonded helical array [25]. For the *cis* rotamer, which is not found in the crystallographic experiment, the geometrical parameters of S_0 state calculated is very similar to those of *trans* rotamer except for different OH orientation. These results indicate that the theoretical methods used in this work should be suitable for the study of *p* isopropylphenol.

3.2. REMPI and UV-UV Hole Burning Spectra

A one-color R2PI spectrum of jet-cooled *p* isopropylphenol recorded in the origin region of the $S_1 \leftarrow S_0$ transition is shown in Fig. 2(a). This spectrum matches very well with the previously reported fluorescence excitation spectrum of *p* isopropylphenol in a supersonic free jet [11]. It is obvious that the origin band structure of *p* isopropylphenol has a clear resolved doublet feature denoted by A and B, which is similar to that of thioanisole isotopomers (C_6H_5S-CH_2D and C_6H_5S-CHD_2) and 3-aminobenzoic acid [28,39]. This result indicates that there are probably two stable rotamers coexisting in the ground state of *p* isopropylphenol. However, at the higher frequency region above 35,800 cm^{-1} the spectral bands are highly congested, and we cannot assign the observed bands to corresponding rotamers directly. Therefore, the UV-UV hole-burning spectroscopy is required to determine the variety of rotamers and identify the vibronic transitions of different rotamers in the R2PI spectrum. Fig. 2(b) and (c) show the hole-burning experimental results by fixing the probe laser to the first two lowest transitions observed at 35578 cm^{-1} and 35,593 cm^{-1}, respectively. Comparing the spectral features between the R2PI and hole-burning spectra, all of the vibronic bands observed in the R2PI spectrum appear in the hole-burning spectra. Thus, it is clearly demonstrated that *p* isopropylphenol has two rotamers in the jet-cooled beam, and the bands observed at 35578 cm^{-1} and 35,593 cm^{-1} are assigned as the $S_1 \leftarrow S_0$ electronic origins of *trans* and *cis* rotamer, respectively. This confirms Hayes's assumption that there may be two rotamers in jet-cooled *p* isopropylphenol [11], and is in line with our DFT and previous MP2

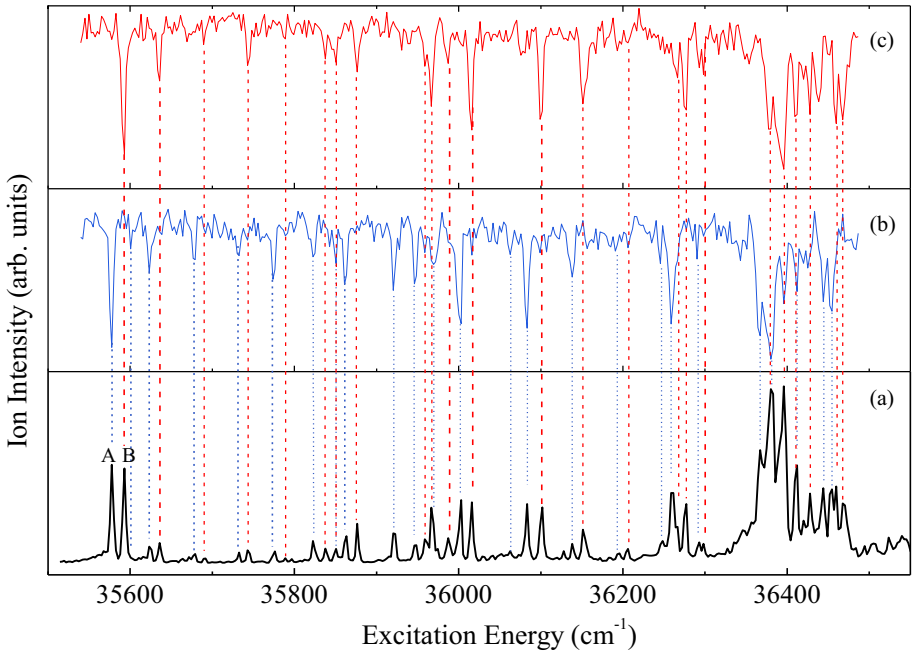

Fig. 2. One-color resonant two-photon ionization (1C-R2PI) spectrum of *p* isopropylphenol (a) and UV-UV hole-burning spectra with the probe laser fixed at 35578 cm^{-1} (b) and 35,593 cm^{-1} (c). The dot and dash lines are used to link the 1C-R2PI bands to the hole-burning spectral bands of *trans* and *cis* rotamers of *p* isopropylphenol, respectively.

[24] theoretical prediction. For the conformational assignment of the electronic origins of the two rotamers, we will explain it in detail in discussion section.

Each rotamer of *p* isopropylphenol has 60 normal modes, including 27 isopropyl, 30 benzenelike and 3 hydroxyl vibronic modes. Generally, of benzene derivatives mainly involves the π electron excitation around the aromatic ring [13], leading to many active vibrations associated with the aromatic ring in the S_1 state. However, only those vibronic bands with sufficiently large Franck-Condon overlaps can be observed in experimental spectrum [40]. In principle, the Franck-Condon simulations of the vibrationally resolved electronic spectra give insight into the vibronic components of the spectral bands, and therefore are used straightforwardly as the basis for assignment of the vibrational bands observed in the experiment [41]. The simulated spectra of both rotamers for the $S_1 \leftarrow S_0$ electronic transition based on the Franck-Condon approximation are presented in Figs. 3 and 4 together with the respective hole-burning spectra. Obviously, the main features of the hole-burning spectra are well reproduced by the simulations. For example, the four main vibronic bands in the experimental spectrum of *trans* rotamer (Fig. 3a) located at 425, 505, 681, and 802 cm^{-1} match well the simulated bands at 430, 515, 689, and 800 cm^{-1} (Fig. 3b), respectively. Similar to the *trans* rotamer, the intense bands at 423, 506, 684, and 803 cm^{-1} in the hole-burning spectrum of *cis* rotamer (Fig. 4a) correspond closely to the simulated spectral bands at 427, 506, 684, and 802 cm^{-1} (Fig. 4b), respectively. In addition, the calculated intensity of the band at 269 cm^{-1} in Fig. 3b is slightly overestimated relative to observed one at 273 cm^{-1}. This may be due to the difference in the calculated geometries of the *trans* rotamers in the S_0 and S_1 states.

Based on such good reproduction of the spectral simulations and the previous spectral assignments on isopropylbenzene [42], *p* isopropylaniline [43], *p* ethylphenol [13], and *p n* propylphenol [15], we can tentatively assign the vibrational bands observed in R2PI spectrum. Table 2 lists the excitation energies, vibrational frequencies, and possible assignments for two rotamers in their S_1 states. The labeling convention of the vibrational modes follows the Varsanyi's system [44], and is based on the Wilson's notation [45]. The strong bands at 425, 505, 681, 802, and 155 cm^{-1} for *trans* rotamer, and 423, 506, 684, 803, and 150 cm^{-1} for *cis* rotamer are assigned to the transitions of $6a_0^1$, $6b_0^1$, 12_0^1, 1_0^1, and $16a_0^1$, respectively. Vibrational modes of 6a, 6b, 12, and 1 mainly involve in-plane ring deformation, whereas mode 16a is associated to out-of-plane ring bending. The fundamental

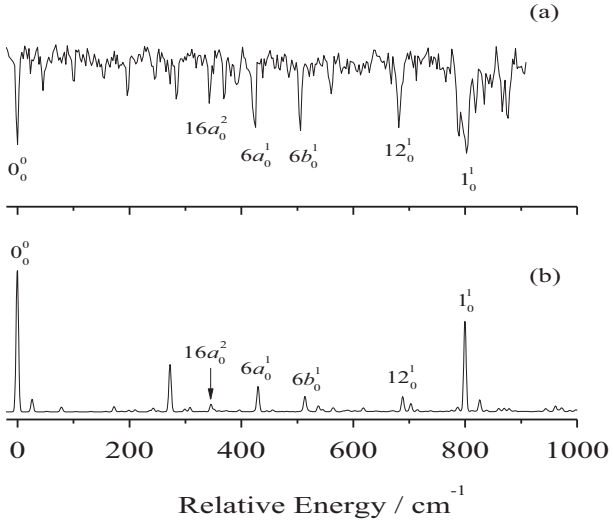

Fig. 3. Comparison of the UV-UV hole-burning spectrum (a) and the Franck-Condon simulation of the $S_1 \leftarrow S_0$ transition (b) of *trans* rotamer.

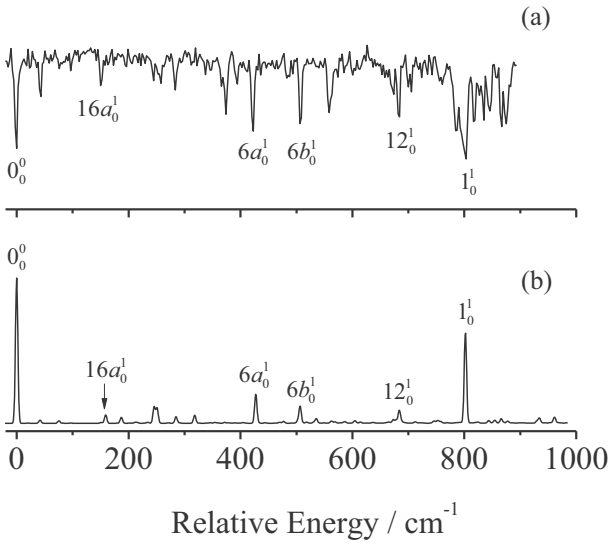

Fig. 4. Comparison of the UV-UV hole-burning spectrum (a) and the Franck-Condon simulation of the $S_1 \leftarrow S_0$ transition (b) of *cis* rotamer.

frequency of substituent-sensitive vibration 9b is 391 cm^{-1} for *trans* rotamer and 394 cm^{-1} for *cis* rotamers, which is related to in-plane bending of C—OH. The low-frequency bands at 23, 45, 244, and 283 cm^{-1} for *trans* rotamer, and at 43, 245, and 283 cm^{-1} for *cis* rotamer are assigned to the vibrations of isopropyl or methyl group. Such modes related to alkyl vibrations have also been previously

Table 2
Transition energies, vibrational frequencies, and the corresponding assignments for REMPI spectrum of *p* isopropylphenol (cm^{-1}).

trans			*cis*			Assignment[b]
Transition energy	Exp.	Calc.[a]	Transition energy	Exp.	Calc.[a]	
35,578	0		35,593	0		0_0^0, band origin
35,601	23	26				$\tau(C_3H_7)$
35,623	45	53	35,636	43	42	$\tau^2(C_3H_7)$
35,677	99	105	35,689	96	97	$11_0^1\tau(C_3H_7)$
35,733	155	173	35,743	150	159	$16a_0^1,\gamma(CCC)$
35,774	196	199				$16a_0^1\tau(C_3H_7)$
35,822	244	243	35,838	245	246	$\tau(CH_3)$
			35,851	258	251	γ(O—H)
35,851	273	269				$\tau(C_3H_7)\delta(C—CH_3)$
35,861	283	273	35,876	283	284	$\delta(C—CH_3)$
35,920	342	346				$16a_0^2,\gamma(CCC)$
35,946	368	372	35,958	366	361	$11_0^1\delta(C—CH_3)$
			35,967	374	378	$10b_0^1 11_0^1$
35,969	391	397	35,987	394	394	$9b_0^1$, β(C—OH)
36,003	425	430	36,016	423	427	$6a_0^1$, β(CCC)
36,083	505	513	36,099	506	506	$6b_0^1$, β(CCC)
36,138	560	538	36,151	558	535	$10a_0^1$, γ(CH)
36,191	613	617	36,206	613	605	$10b_0^2$
36,247	669	673	36,266	673	673	$6a_0^1\tau(CH_3)$
36,259	681	689	36,277	684	684	12_0^1, β(CCC)
			36,298	705	712	$6a_0^1\delta(C—CH_3)$
36,290	712	715				$12_0^1\tau(C_3H_7)$
36,367	789	786	36,378	785		$6b_0^1\gamma(O—H)$
36,380	802	800	36,396	803	802	1_0^1, breathing
36,396	818		36,410	817	824	$6b_0^1 16a_0^2$
36,412	834	826	36,428	835	843	$1_0^1\tau(C_3H_7)$
36,425	847	860	36,439	846	855	$6a_0^2$,β(CCC)
36,444	866	870	36,460	867	866	$\nu(C—CH_3)$
36,454	876	879	36,468	875	877	$1_0^1 11_0^1$

[a] The calculated values are obtained from the TD-B3LYP/aug-cc-pVDZ calculations, scaled by 0.9902 and 0.9845 for *trans* and *cis* rotamers, respectively.
[b] ν, stretching; β, in-plane bending; γ, out-of-plane bending; τ, torsion; δ, alkyl bending.

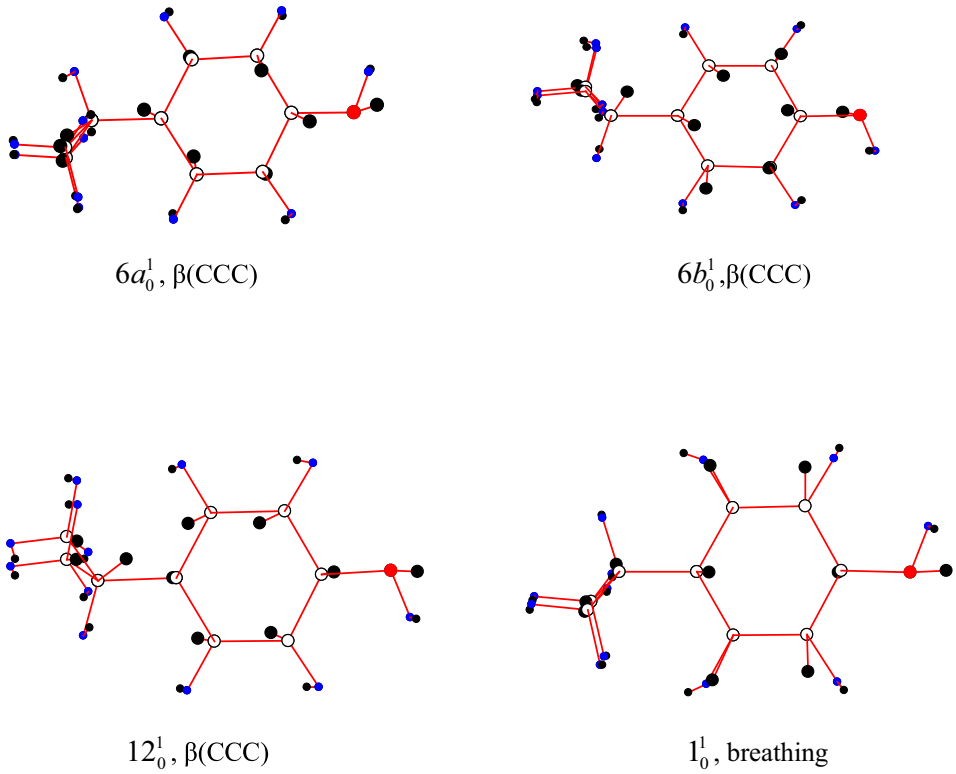

Fig. 5. Some active vibrational modes of *trans* rotamer of *p* isopropylphenol in its S_1 state. The open circles mark the original positions of the atoms, whereas the solid dots indicate the displaced positions.

observed in the toluene [46,47], *p* methylphenol [11,13], *p* ethylphenol [13], *p n* propylphenol [15], and acetaminophen [29]. The vibrational patterns of several intense normal modes of *trans* rotamer observed in R2PI spectrum are shown in Fig. 5, while those of *cis* rotamer are similar and not shown repeatedly. In addition, the superposition of the *trans* and *cis* FC simulations is also compared to the R2PI spectrum of *p* isopropylphenol, as shown in Fig. S1. Although the relative intensities of the bands in the simulated spectrum show some deviations from the R2PI spectrum, the main spectral features of the experimental spectrum are reproduced, especially the vibrational modes 6a, 6b, 12 and 1 of these two rotamers.

It is worth noting that the observed vibrational modes and corresponding frequencies of *trans* rotamer are nearly identical to those of *cis* rotamer, which means that both rotamers exhibit similar spectral features. Meanwhile, the energy difference between the origin bands of *trans* and *cis* rotamers is 15 cm^{-1}, which is also almost identical to the energy differences between other same transitions of two rotamers (Table 2). These results indicate the similarity of the two rotamers in structures, and that the intramolecular coupling interaction between hydroxyl group and isopropyl group can be ignored due to long distance. As a consequence, the slight difference between the vibrational features of both rotamers is not sufficiently sensitive to make the conformational assignment of two rotamers [48]. Due to the insensitivity of the vibrational frequencies to the molecular conformation, the vibrational bands of the *trans* and *cis* rotamers observed in the S_0 state are likely to be overlapping. This could be used in part to explain the neglect of the presence of the *cis*-rotomer in the infrared spectroscopy of *p* isopropylphenol (in the solid phase and in solution) [22]. In addition, the R2PI spectrum in the higher frequency region is quite congested, resulting from the heavy overlap of different vibrations between two rotamers. As shown in Fig. 2, the band at 36396 cm^{-1} is an overlap of $6b_0^1 16a_0^2$ transition of *trans* rotamer and 1_0^1 transition of *cis* rotamer.

3.3. Cation Spectra

To gain insight into the information of *p* isopropylphenol in the cationic ground D_0 state, we perform the photoionization efficiency (PIE) and MATI experiments. The PIE signal involves the prompt ions and threshold ions, and it is more sensitive than that of MATI [49]. Therefore we performed PIE experiments before the MATI work. The PIE curves of *trans* and *cis* rotamers of *p* isopropylphenol via their origins of S_1 state are shown in Fig. S2. The rising steps give the adiabatic IEs of 65,331 ± 10 cm^{-1} and 65,354 ± 10 cm^{-1} for *trans* and *cis* rotamers, respectively. In comparison with PIE experiment, the MATI experiment only detects the threshold ions produced by field-ionizing Rydberg neutrals, which gives a sharp peak in the MATI spectrum, and a more precise value of the IE is obtained. Fig. 6a and 7a display the MATI spectra of *trans* and *cis* rotamers of *p* isopropylphenol via the origins of S_1 state, respectively. The most intense peaks in the two spectra correspond to the origins of $D_0 \leftarrow S_1$ transition of two rotamers. The resulting adiabatic IEs are 65,331 ± 5 cm^{-1} (8.1000 ± 0.0006 eV) and 65,350 ± 5 cm^{-1} (8.1024 ± 0.0006 eV) for *trans* and *cis* rotamers, respectively, which include the correction for Stark effect due to pulsed electronic field [50]. The distinctive IEs from PIE and MATI experiments also confirm the existence of the two rotamers of *p* isopropylphenol.

MATI technique can precisely measure the active vibrations of molecule in the D_0 state. Fig. 6 shows the MATI spectra of *trans* rotamer via $S_1 0^0$ state together with the corresponding Franck-Condon simulation. It is evident that the simulated spectra are in qualitative agreement with the experimental results, which can help us to assign the observed MATI bands. The simulated spectral profile and experimental spectra are dominated by the 0–0 transitions. The simulated vibrations at 189 cm^{-1} (δ(C—C_3H_7)), 824 cm^{-1} (1^1), 862 cm^{-1} ($17b^1$), 1182 cm^{-1} ($9a^1$), 1215 cm^{-1} (ν(C—C_3H_7)), and 1658 cm^{-1} ($8a^1$) should correspond to the experimental bands located at 198, 824, 865,1178,1220,

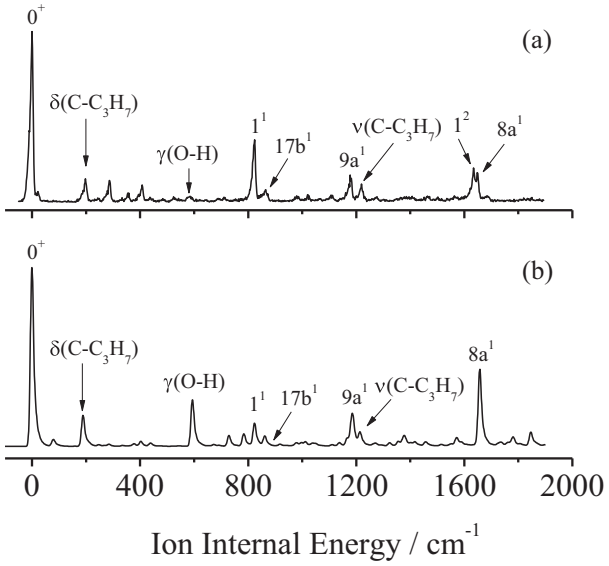

Fig. 6. Comparison of the experimental MATI spectrum recorded via the electronic origin of the S_1 state (a) and its Franck-Condon simulation (b) for *trans* rotamer.

and 1648 cm^{-1}, respectively. The weak band observed at 585 cm^{-1} matches well the calculated frequency of mode γ(O—H) (594 cm^{-1}), but its intensity is overestimated in the simulation. Additionally, in the spectral region between 1600 and 1700 cm^{-1}, two intense bands assigned as modes 1^2 and $8a^1$ can be observed in the experiment, whereas only mode $8a^1$ has an intense intensity in the simulated MATI spectrum. This could be attributed to a Fermi resonance effect between mode 1^2 and mode $8a^1$, which are not taken into account in our simulation [41,51]. As shown in Fig. 7, the main vibrational bands of *cis* rotamer in MATI spectrum located at 201, 288, 824, 866, 1178, 1218, 1652 cm^{-1}, are in line with the simulated ones at 201 cm^{-1} (δ(C—C_3H_7)), 285 cm^{-1} (δ(C—CH_3)), 824 cm^{-1} (1^1), 862 cm^{-1} ($17b^1$), 1180 cm^{-1} ($9a^1$), 1217 cm^{-1} (ν(C—C_3H_7)), and 1656 cm^{-1} ($8a^1$), respectively. Similar to MATI spectrum of *trans* rotamer, a Fermi

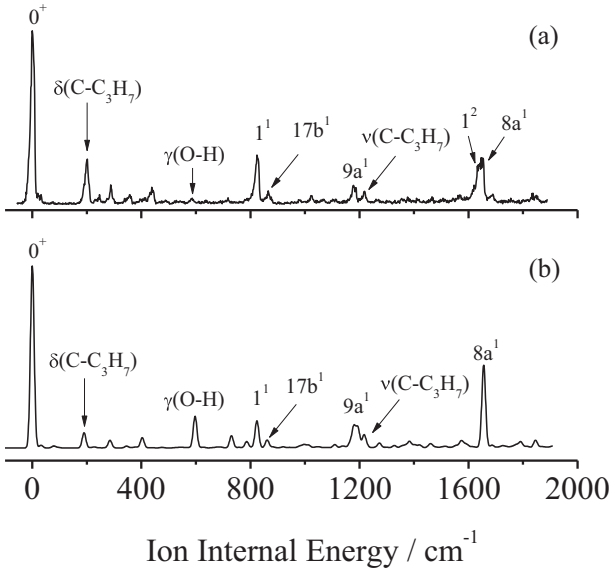

Fig. 7. Comparison of the experimental MATI spectrum recorded via the electronic origin of the S_1 state (a) and its Franck-Condon simulation (b) for *cis* rotamer.

resonance between mode 1^2 and mode $8a^1$ are found in MATI spectrum of *cis* rotamer as well. All the observed vibrational features of *trans* and *cis* rotamers in the D_0 state are summarized in Tables 3 and 4, including the experimental and calculated vibrational frequencies, and possible assignments. Most of intense vibrations of the two rotamers in the D_0 state correspond to the in-plane ring deformation as well as some active modes involving isopropyl group.

The MATI spectra of *trans* and *cis* rotamers via the $S_1 6a^1$ and $S_1 6b^1$ intermediate states are shown in Figs. 8 and 9, respectively. The most prominent feature of all the MATI spectra is that the strongest vibrational band corresponds to the same vibrational mode as the intermediate state. The $\Delta v = 0$ propensity rule of maintaining a strong correlation of the same vibrations between the excited and cationic states has been reported in previous studies of substituted aromatic molecules [13,51–55]. Therefore, when the $S_1 6a^1$ and $S_1 6b^1$ states are used as the intermediate states, most of bands in the MATI spectra can be assigned as combination bands involving $6a^1$ and $6b^1$ vibrations, as seen in Figs. 8 and 9. The MATI bands in the low frequency region (<400 cm^{-1}) are related to isopropyl vibrations, as shown in Figs. 6a and 7a. However, these bands are absent in the MATI spectra via the intermediate states $S_1 6a^1$ and $S_1 6b^1$, which implies the very weak coupling between isopropyl group and the aromatic ring upon ionization. It is interesting to notice that the ring breathing vibration 1^1 is the most intense in R2PI spectrum, and it is also observable in the form of fundamental and combination bands in the MATI spectra.

Table 3
Observed vibrational frequencies (in cm^{-1}) and assignments in the MATI spectra of *p* isopropylphenol (*trans* rotamer).

Intermediate level in the S_1 state[a]			Calc.[a]	Assignment[b]
0^0	$6a^1$	$6b^1$		
198			189	δ(C—C_3H_7)
243			248	τ(CH_3)
286			285	δ(C—CH_3)
355			364	$16a^1$, γ(CCC)
407			403	$9b^1$, β(C–OH)
436	436		438	$6a^1$, β(CCC)
524		528	527	$6b^1$, β(CCC)
585	587	595	594	γ(O—H)
	638			$6a^1$δ(C—C_3H_7)
715	724	724	729	$16a^2$, γ(CCC)
790			786	$10a^1$, γ(CH)
		816		$6b^1$δ(C—CH_3)
824			824	1^1, breathing
	840			$6a^1 9b^1$
865			862	$17b^1$, γ(CH)
	875	880		$6a^2$
		937		$6b^1 9b^1$
980			982	5^1, γ(CH)
1020			1013	1^1δ(C—C_3H_7)
1107			1109	1^1δ(C—CH_3)
1178			1182	$9a^1$, β(CH)
1220			1215	ν(C—C_3H_7)
	1260			$6a^1 1^1$
1276			1274	3^1, β(CH)
	1305			$6a^3$
		1351		$6b^1 1^1$
		1392		$6b^1 17b^1$
	1417			$6a^1 5^1$
1463	1457		1456	$17b^1$γ(O—H)
1563	1548		1572	$10a^2$
	1617			$6a^1 9a^1$
1634			1648	1^2
1648	1650		1658	$8a^1$, ν(CC)
1685				$8a^1$τ(C_3H_7)
		1705		$6b^1 9a^1$
		1744		$6b^1$ν(C—C_3H_7)

[a] The experimental values are shifts from 65,331cm^{-1}, whereas the predicted ones are obtained from the B3LYP/aug-cc-pVDZ calculations, scaled by 0.9896.
[b] ν, stretching; β, in-plane bending; γ, out-of-plane bending; τ, torsion; δ, alkyl bending.

Table 4
Observed vibrational frequencies (in cm^{-1}) and assignments in the MATI spectra of *p* isopropylphenol (*cis* rotamer).

Intermediate level in the S_1 state[a]			Calc.[a]	Assignment[b]
0^0	$6a^1$	$6b^1$		
201			190	δ(C—C_3H_7)
246			248	τ(CH_3)
288			285	δ(C—CH_3)
345			346	$10b^1$τ(C_3H_7)
357			365	$16a^1$, γ(CCC)
411			403	$9b^1$, β(C—OH)
438	437	431	438	$6a^1$, β(CCC)
528	538	532	527	$6b^1$, β(CCC)
587	599		597	γ(O—H)
	635			$6a^1$δ(C—C_3H_7)
		689		$9b^1$δ(C—CH_3)
718	727	733	731	$16a^2$, γ(CCC)
787			786	$10a^1$, γ(CH)
824			824	1^1, breathing
	834			$6a^19b^1$
866			862	$17b^1$, γ(CH)
	876			$6a^2$
1022			1014	1^1δ(C—C_3H_7)
1178			1180	$9a^1$, β(CH)
1218			1217	ν(C—C_3H_7)
1270			1273	3^1, β(CH)
	1262			$6a^11^1$
	1303			$6a^3$
		1354		$6b^11^1$
		1386		$6b^117b^1$
1465	1465		1459	$17b^1$γ(O—H)
1561	1549		1573	$10a^2$
	1618			$6a^19a^1$
1640			1648	1^2
1652	1654		1656	$8a^1$, ν(CC)
1689			1688	$8a^1$τ(C_3H_7)
		1715		$6b^19a^1$
		1748		$6b^1$ν(C—C_3H_7)
1849			1846	$8a^1$δ(C—C_3H_7)

[a] The experimental values are shifts from 65,350 cm^{-1}, whereas the predicted ones are obtained from the B3LYP/aug-cc-pVDZ calculations, scaled by 0.9891.
[b] ν, stretching; β, in-plane bending; γ, out-of-plane bending; τ, torsion; δ, alkyl bending.

4. Discussion

According to our calculations at B3LYP/aug-cc-pVDZ level, the *trans* rotamer is slightly more stable than the *cis* rotamer in the S_0 state and the energy difference of both rotamers is 16 cm^{-1} with zero-point energy correction. Additionally, the energy barrier between *trans* and *cis* rotamers calculated by rotating the hydroxyl group (Fig. S3) is 1240 cm^{-1}. This value is consistent with the experimental one of 1215 cm^{-1} in phenol for hydroxyl rotation [56]. Ruoff et al. have demonstrated that if the interconversion barrier between rotamers is greater than about 400 cm^{-1}, in the supersonic expansion the conformational relaxation will not happen [57]. Here the barriers of 1240 cm^{-1} are sufficiently high to avoid the conformational relaxation, thus the two rotamers of *p* isopropylphenol can coexist in the molecular beam.

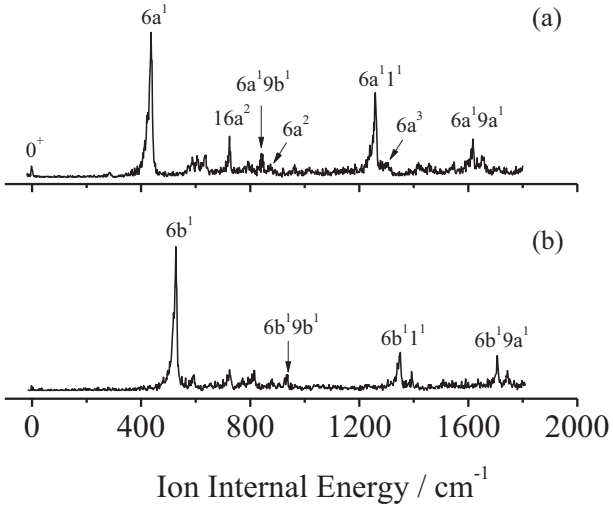

Fig. 8. MATI spectra of *trans* rotamer via the following vibrational levels of the S_1 state as intermediate states: (a) $6a^1$ and (b) $6b^1$.

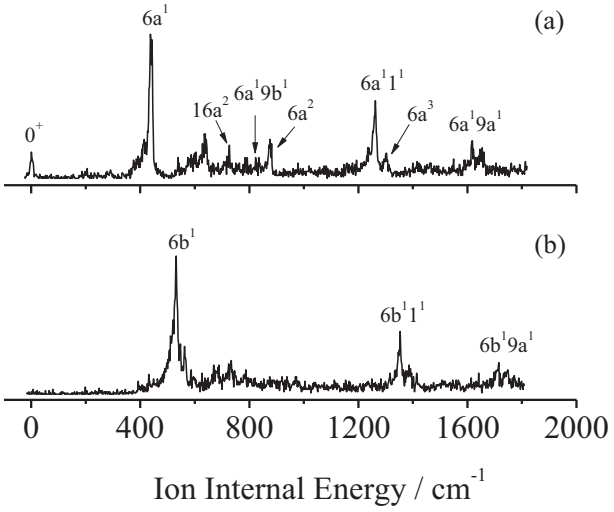

Fig. 9. MATI spectra of *cis* rotamer via the following vibrational levels of the S_1 state as intermediate states: (a) $6a^1$ and (b) $6b^1$.

It is well known that the relative intensities of the origin bands for different rotamers depend mainly on the population of the electronic ground state and the oscillator strengths for the $S_1 \leftarrow S_0$ electronic transition [35,57,58]. Therefore, the ratio (I_A/I_B) of intensities of the A and B bands in the R2PI spectrum displayed in Fig. 2 can directly reflect the relative abundance of the two rotamers at the nozzle temperature (373 K in our experiment), due to the same oscillator strength of the two rotamers predicted in our TDDFT calculations. In addition, because of a high energy barrier between the *trans* and *cis* rotamers, the conformational interchange could not significantly occur during the expansion. Thus, the relative abundance of the *trans* and *cis* rotamers in the molecular beam is approximately the same as that in the nozzle. Furthermore, we can use the following expression to evaluate the relative energy of rotamers in the S_0 state: $I_A/I_B = \exp(-\Delta E/KT)$, where ΔE is the energy difference between the two rotamers, and T is the temperature of the nozzle [57,59]. Using the ratio I_A/I_B gives a value of ΔE_{A-B} of -9.7 cm^{-1}. This is in good agreement with the theoretical energy difference of -16 cm^{-1} between the *trans* and *cis* rotamer in the S_0 state. On the other hand, we perform TD-B3LYP/aug-cc-pVDZ calculations for the S_1 state and B3LYP/aug-cc-pVDZ calculations for the S_0 state of *p* isopropylphenol and found that the calculated adiabatic excitation energy of *trans* rotamer is about 13 cm^{-1} lower than that of *cis* rotamer. The band A shows a redshift of 15 cm^{-1} compared to the band B in the R2PI experiment. These results enable us to assign the band A to origin of *trans* rotamer and the band B to origin of *cis* rotamer. A further confirmation of this assignment comes from the comparison of the excited energies between *trans* and *cis* rotamers of *p* methoxyphenol and *p* ethoxyphenol. For these two molecules, *trans* rotamer has a lower excited energy than *cis* rotamer [60,61], which is consistent with *p* isopropylphenol, as listed in Table S2.

On the basis of our calculations, the first electronically excited state S_1 for the two rotamers of *p* isopropylphenol is mainly dominated by the LUMO ← HOMO excitation. During the $S_1 \leftarrow S_0$ transition of both rotamers, all C—C bond lengths of the ring are slightly increased by

0.025 Å on average, while the bond lengths of C_1O_{11} and C_4—C_8 decrease, as listed in Table 1. Other geometric changes are related to the extension of the $C_3C_4C_5$ and $C_6C_1C_2$ angles. These changes are in line with the π electron excitation of the aromatic ring and a decrease of the electron density on the oxygen atom and isopropyl group upon excitation. This could be the reason for the intense bands of the ring breathing mode 1 and in-plane ring deformation modes 6a, 6b and 12 in the R2PI spectrum of *p* isopropylphenol. In previous studies of phenol [62] and anisole [41], similar structural changes related to C—C bonds of aromatic ring and C—O bond can also be found.

For the MATI spectra of *p* isopropylphenol, a strong propensity of $\Delta\upsilon = 0$ mentioned in Section 3.3 indicates the molecular geometry of cation in the D_0 state resemble those of the neutral species in the S_1 state for *trans* and *cis* rotamers. This is further verified by comparing the calculated structures between the S_1 and D_0 state for each rotamer. The overall change of the aromatic ring in size is within 0.8% upon ionization (Table S1). Although the molecular structures of the two rotamers are similar during the $D_0 \leftarrow S_1$ transition, it leads to notable variations in the vibrational frequencies. The in-plane ring deformation modes 9b, 6a, 6b, and 1 of *trans* rotamer are observed at 391, 425, 560, and 802 cm^{-1} in the S_1 state and 407, 436, 595, and 824 cm^{-1} in the D_0 state. Similar to *trans* rotamer, the modes 9b, 6a, 6b, and 1 of *cis* rotamer are observed at 394, 423, 558, and 803 cm^{-1} in the S_1 state and 411, 437, 587, and 824 cm^{-1} in the D_0 state. It is obvious that frequencies of these vibrations in the D_0 state are buleshifted from those in the S_1 state. Because the vibrational frequency reflects the rigidity of the chemical bond related to the corresponding vibration, the increase of the vibrational frequencies suggests that the bond strength of the ring is stronger in the cationic D_0 state than in the neutral S_1 state.

5. Conclusion

We have performed the 1C-R2PI, UV-UV hole burning and MATI spectroscopy for the first time to study the vibrational spectra of *p* isopropylphenol in the first electronically excited state S_1 and cationic ground state D_0. The UV-UV hole burning spectroscopy reveals the presence of two stable rotamers of *p* isopropylphenol in the supersonic molecular beam. With the aid of quantum chemical calculations, the structures of the two rotamers are assigned to the *trans* and *cis* forms and the former is slightly more stable in the ground S_0 state than the latter. Because of their structural similarity, the two rotamers exhibit similar spectral features in the S_1 state. The electronic excitation energies E_1 of $S_1 \leftarrow S_0$ transition are determined to be 35,578 and 35,593 cm^{-1} for *trans* and *cis* rotamers, respectively. The vibronic bands of the R2PI spectrum at high frequency region of 36,350–36,420 cm^{-1} are congested and more intense than the origin bands. This is caused by the overlaps of several vibronic bands of the two rotamers, which can be confirmed by our hole-burning spectra. The accurate ionization energies are determined to be 65,331 ± 5 cm^{-1} (8.1000 ± 0.0006 eV) and 65,350 ± 5 cm^{-1} (8.1024 ± 0.0006 eV) for *trans* and *cis* rotamers, respectively. The MATI spectra of *p* isopropylphenol obtained via different intermediate levels of S_1 state show a propensity rule of $\Delta\upsilon = 0$, and indicate the similarity in the molecular geometry between the S_1 state and the D_0 state for each rotamer of *p* isopropylphenol. The in-plane deformation vibrations 9b, 6a, 6b, and 1 of both rotamers have higher frequencies in the D_0 state than in the S_1 state, suggesting the stronger bond strength of the ring in the D_0 state. The detailed vibronic features of *p* isopropylphenol in S_1 and D_0 states could help us to understand photochemical and photophysical properties of phenol and their derivatives.

Acknowledgments

This work was supported by National Key R&D Program of China (Grant No. 2017YFA0304203), PCSIRT (No. IRT_17R70), National Natural Science Foundation of China (Grants Nos. 61575115, 61378039, 61378049, 11434007), 111 Project (Grant No. D18001), the Construction of State Key Laboratory of Quantum Optics and Quantum Optics Devices, China (Grant No. 2015012001-20), and the Fund for Shanxi"1331 Project" Key Subjects Construction.

Appendix A. Supplementary data

Supplementary data to this article can be found online at https://doi.org/10.1016/j.saa.2018.09.013.

References

[1] T.N.V. Karsili, A.M. Wenge, S.J. Harris, D. Murdock, J.N. Harvey, R.N. Dixon, M.N.R. Ashfold, Chem. Sci. 4 (2013) 2434–2446.
[2] G.A. King, A.L. Devine, M.G.D. Nix, D.E. Kelly, M.N.R. Ashfold, Phys. Chem. Chem. Phys. 10 (2008) 6417–6429.
[3] G.A. Pino, A.N. Oldani, E. Marceca, M. Fujii, S.-I. Ishiuchi, M. Miyazaki, M. Broquier, C. Dedonder, C. Jouvet, J. Chem. Phys. 133 (2010), 124313.
[4] T.N.V. Karsili, A.M. Wenge, B. Marchetti, M.N.R. Ashfold, Phys. Chem. Chem. Phys. 16 (2014) 588–598.
[5] M. Miyazaki, Y. Sakata, M. Schutz, O. Dopfer, M. Fujii, Phys. Chem. Chem. Phys. 18 (2016) 24746–24754.
[6] E. Fujimaki, A. Fujii, T. Ebata, N. Mikami, J. Chem. Phys. 112 (2000) 137–148.
[7] R.A. Livingstone, J.O.F. Thompson, M. Iljina, R.J. Donaldson, B.J. Sussman, M.J. Paterson, D. Townsend, J. Chem. Phys. 137 (2012), 184304.
[8] M.N.R. Ashfold, G.A. King, D. Murdock, M.G.D. Nix, T.A.A. Oliver, A.G. Sage, Phys. Chem. Chem. Phys. 12 (2010) 1218–1238.
[9] M.N.R. Ashfold, A.L. Devine, R.N. Dixon, G.A. King, M.G.D. Nix, T.A.A. Oliver, Proc. Natl. Acad. Sci. 105 (2008) 12701–12706.
[10] S.J. Martinez, J.C. Alfano, D.H. Levy, J. Mol. Spectrosc. 137 (1989) 420–426.
[11] K. Song, J.M. Hayes, J. Mol. Spectrosc. 134 (1989) 82–97.
[12] S.J. Martinez, J.C. Alfano, D.H. Levy, J. Mol. Spectrosc. 152 (1992) 80–88.
[13] J.L. Lin, C. Li, W.B. Tzeng, J. Chem. Phys. 120 (2004) 10513–10519.
[14] G. Myszkiewicz, W.L. Meerts, C. Ratzer, M. Schmitt, J. Chem. Phys. 123 (2005) 044304.
[15] C. Li, J.L. Lin, W.B. Tzeng, J. Chem. Phys. 122 (2005) 044311.
[16] M. Gerhards, B. Kimpfel, M. Pohl, M. Schmitt, K. Kleinermanns, J. Mol. Struct. 270 (1992) 301–324.
[17] A.N. Oldani, J.C. Ferrero, G.A. Pino, Phys. Chem. Chem. Phys. 11 (2009) 10409–10416.
[18] F.J. Hernandez, M.C. Capello, A.N. Oldani, J.C. Ferrero, P. Maitre, G.A. Pino, Phys. Chem. Chem. Phys. 14 (2012) 8945–8955.
[19] Y. Liu, C. Zhang, Y. Yang, D. Yang, D. Shi, J. Sun, J. Clust. Sci. 23 (2012) 1029–1038.
[20] M.C. Capello, F.J. Hernandez, M. Broquier, C. Dedonder-Lardeux, C. Jouvet, G.A. Pino, Phys. Chem. Chem. Phys. 18 (2016) 31260–31267.
[21] A. Fujii, E. Fujimaki, T. Ebata, N. Mikami, Chem. Phys. Lett. 303 (1999) 289–294.
[22] M.M. Szostak, T. Misiaszek, S. Roszak, J.G. Rankin, R.S. Czernuszewicz, J. Phys. Chem. 99 (1995) 14992–15003.
[23] G. Wojcik, J. Holband, Acta Cryst. B 58 (2002) 684–689.
[24] P.R. Richardson, M.A. Chapman, D.C. Wilson, S.P. Bates, A.C. Jones, Phys. Chem. Chem. Phys. 4 (2002) 4910–4915.
[25] M. Perrin, C. Bavoux, A. Thozet, Acta Cryst. B 33 (1977) 3516–3520.
[26] A. Min, A. Ahn, C.J. Moon, J.H. Lee, Y.G. Seong, S.K. Kim, M.Y. Choi, Phys. Chem. Chem. Phys. 19 (2017) 4840–4848.
[27] N. Mayorkas, H. Sachs, M. Schutz, S.-i. Ishiuchi, M. Fujii, O. Dopfer, I. Bar, Phys. Chem. Chem. Phys. 18 (2016) 1191–1201.
[28] J. Lee, S.-Y. Kim, S.K. Kim, J. Phys. Chem. A 118 (2014) 1850–1857.
[29] W.Y. Sohn, S.-i. Ishiuchi, M. Miyazaki, J. Kang, S. Lee, A. Min, M.Y. Choi, H. Kang, M. Fujii, Phys. Chem. Chem. Phys. 15 (2013) 957–964.
[30] M. Haruhiko, M. Mitsuhiko, B.N. Iben, C. Pierre, D. Claude, J. Christophe, I. Shun-ichi, F. Masaaki, J. Phys. Chem. Lett. 1 (2010) 1130–1133.
[31] L. Zhu, P. Johnson, J. Chem. Phys. 94 (1991) 5769–5771.
[32] C.E.H. Dessent, K. Müller-Dethlefs, Chem. Rev. 100 (2000) 3999–4022.
[33] K. Müller-Dethlefs, E.W. Schlag, Angew. Chem. Int. Ed. 37 (1998) 1346–1374.
[34] Y. Jin, Y. Zhao, Y. Yang, L. Wang, C. Li, S. Jia, Chem. Phys. Lett. 692 (2018) 395–401.
[35] S.J. Lee, A. Min, Y. Kim, A. Ahn, J. Chang, S.H. Lee, M.Y. Choi, S.K. Kim, Phys. Chem. Chem. Phys. 13 (2011) 16537–16541.
[36] M.J. Frisch, G.W. Trucks, H.B. Schlegel, G.E. Scuseria, M.A. Robb, J.R. Cheeseman, J.A. Montgomery Jr., T. Vreven, K.N. Kudin, J.C. Burant, J.M. Millam, S.S. Iyengar, J. Tomasi, V. Barone, B. Mennucci, M. Cossi, G. Scalmani, N. Rega, G.A. Petersson, H. Nakatsuji, M. Hada, M. Ehara, K. Toyota, R. Fukuda, J. Hasegawa, M. Ishida, T. Nakajima, Y. Honda, O. Kitao, H. Nakai, M. Klene, X. Li, J.E. Knox, H.P. Hratchian, J.B. Cross, V. Bakken, C. Adamo, J. Jaramillo, R. Gomperts, R.E. Stratmann, O. Yazyev, A.J. Austin, R. Cammi, C. Pomelli, J.W. Ochterski, P.Y. Ayala, K. Morokuma, G.A. Voth, P. Salvador, J.J. Dannenberg, V.G. Zakrzewski, S. Dapprich, A.D. Daniels, M.C. Strain, O. Farkas, D.K. Malick, A.D. Rabuck, K. Raghavachari, J.B. Foresman, J.V. Ortiz, Q. Cui, A.G. Baboul, S. Clifford, J. Cioslowski, B.B. Stefanov, A.G. Liu, Gaussian 09, Revision C.01, Gaussian, Inc., Wallingford CT, 2009.
[37] J.P. Merrick, D. Moran, L. Radom, J. Phys. Chem. A 111 (2007) 11683–11700.
[38] P. Sinha, S.E. Boesch, C. Gu, R.A. Wheeler, A.K. Wilson, J. Phys. Chem. A 108 (2004) 9213–9217.
[39] Y. He, C. Wu, W. Kong, J. Chem. Phys. 121 (2004) 8321–8328.
[40] J.L. Lin, S. Zhang, W.B. Tzeng, J. Chem. Phys. 120 (2004) 5057–5063.
[41] J. Bloino, M. Biczysko, O. Crescenzi, V. Barone, J. Chem. Phys. 128 (2008) 244105.

[42] J.B. Hopkins, D.E. Powers, R.E. Smalley, J. Chem. Phys. 72 (1980) 5039–5048.
[43] D.E. Powers, J.B. Hopkins, R.E. Smalley, J. Chem. Phys. 72 (1980) 5721–5730.
[44] G. Varsanyi, Assignments of Vibrational Spectra of Seven Hundred Benzene Derivatives, Wiley, New York, 1974.
[45] E.B. Wilson, Phys. Rev. 45 (1934) 706–714.
[46] P.J. Breen, J.A. Warren, E.R. Bernstein, J.I. Seeman, J. Chem. Phys. 87 (1987) 1917–1926.
[47] C.G. Hickman, J.R. Gascooke, W.D. Lawrance, J. Chem. Phys. 104 (1996) 4887–4901.
[48] M. Schneider, M. Wilke, M.-L. Hebestreit, J.A. Ruiz-Santoyo, L. Alvarez-Valtierra, J.T. Yi, W.L. Meerts, D.W. Pratt, M. Schmitt, Phys. Chem. Chem. Phys. 19 (2017) 21364–21372.
[49] W.B. Tzeng, J.L. Lin, J. Phys. Chem. A 103 (1999) 8612–8619.
[50] B. Zhang, C. Li, H. Su, J.L. Lin, W.B. Tzeng, Chem. Phys. Lett. 390 (2004) 65–70.
[51] S. Kruger, J. Grotemeyer, Phys. Chem. Chem. Phys. 18 (2016) 7100–7113.
[52] S. Krueger, F. Witte, J. Helfrich, J. Grotemeyer, RSC Adv. 5 (2015) 937–948.
[53] C. Harthcock, J. Zhang, W. Kong, Chem. Phys. Lett. 556 (2013) 23–28.
[54] Y. He, C. Wu, W. Kong, J. Chem. Phys. 120 (2004) 7497–7504.
[55] L.J. Zhang, S. Liu, M. Cheng, Y.K. Du, Q.H. Zhu, J. Phys. Chem. A 120 (2016) 81–94.
[56] G. Berden, W.L. Meerts, M. Schmitt, K. Kleinermanns, J. Chem. Phys. 104 (1996) 972–982.
[57] R.S. Ruoff, T.D. Klots, T. Emilsson, H.S. Gutowsky, J. Chem. Phys. 93 (1990) 3142–3150.
[58] X. Tong, M.S. Ford, C.E.H. Dessent, K. Müller-Dethlefs, J. Chem. Phys. 119 (2003) 12908–12913.
[59] V.P. Manea, K.J. Wilson, J.R. Cable, J. Am. Chem. Soc. 119 (1997) 2033–2039.
[60] C. Li, H. Su, W.B. Tzeng, Chem. Phys. Lett. 410 (2005) 99–103.
[61] Z. Qiu-sha, I.F. Teng, Z. Bing, T. Wen Bih, Chin. J. Chem. Phys. 22 (2009) 649.
[62] S. Schumm, M. Gerhards, K. Kleinermanns, J. Phys. Chem. A 104 (2000) 10648–10655.